Tutorial on Wavenumber Transforms of Structural Vibration Fields

Stephen A. Hambric [a)]
Hambric Acoustics, LLC

Andrew R. Barnard [b)]
Penn State University

ABSTRACT

While most new vibro-acousticians quickly understand time-frequency Fourier transforms, learning the similar concept of space-wavenumber transforms is more difficult. Two features of spatial Fourier transforms complicate the learning process: spatial transforms are over two dimensions (time is one dimensional) and negative wavenumber terms are important (negative frequencies are ignored in time-frequency transforms). In this tutorial, we try to demystify spatial Fourier transforms using examples of flat rectangular panel vibration fields which include positive and negative two dimensional wavenumber terms. We also demonstrate the well-known wavenumber filtering approach to eliminate subsonic components of a vibration field, thereby revealing the supersonic radiating vibration field. Finally, we show how wavenumber filtering of measured vibration fields may be used to determine structure-borne transmission coefficients between two panels bolted along a common edge.

1 INTRODUCTION

Structural vibration fields are comprised of many waves of varying amplitude and speed. These wavefields may be decomposed into their individual components using wavenumber transforms. The wavenumber transforms may then be analyzed to calculate quantities like radiated sound, structure-borne sound transmission coefficients, and responsiveness to various forcing functions, such as turbulent flow fields. While amazingly useful, we have found that many beginning vibro-acousticians have difficulty understanding the transform procedures, and the resulting transforms themselves. We therefore offer this tutorial to demystify spatial wavenumber transforms of structural vibration fields.

This paper continues a series on vibro-acoustics tutorials initiated in Acoustics Today magazine [1,2], and continued at Internoise conferences [3,4]. We therefore omit details of basic vibroacoustic analyses in this paper, referring readers to the previous articles.

[a)] email: hambricacoustics@gmail.com
[b)] email: barnard@psu.edu

2 ONE-DIMENSIONAL TRANSFORMS

2.1 Solution of the Wave Equation and Selection of Time Dependence

Education in vibration and acoustics begins with the wave equation. For the purpose of this tutorial, the linear compressional wave equation is a good starting point, although this discussion holds for any variant of the wave equation. The linear compressional wave equation is

$$\nabla^2 f(\vec{r},t) = \frac{1}{c^2}\frac{\partial^2 f(\vec{r},t)}{\partial t^2} \tag{1}$$

where $f(\vec{r},t)$ is a space- and time-dependent quantity such as vibrational displacement or acoustic pressure, and *c* is the speed of sound in the medium. Time-harmonic behavior is represented in the functional form of either $\tilde{f}(\omega t - k\vec{r})$ or $\tilde{f}(k\vec{r} - \omega t)$ where $\tilde{f}$ is a representative solution function, ω is angular frequency, *t* is time, *k* is the wavenumber, defined as ω/c, and $\vec{r}$ is a vector in the solution space, for example [*x, y*] in Cartesian coordinates. Throughout this tutorial, the solution function in the form of $\tilde{f}(\omega t - k\vec{r})$ is chosen which results in a time harmonic function

$$e^{j\omega t} \tag{2}$$

where *j* is the imaginary number $\sqrt{-1}$. The choice of sign of the exponent in the time harmonic function (+*j* vs -*j*) seems innocuous; however, it is extremely important in defining the Fourier transform pairs and in separating outward and inward traveling waves in the wavenumber domain. Using this sign convention for time-harmonic behavior, Equation 2 can be substituted into Equation 1 and the result differentiated to produce the homogeneous[1] Helmholtz Equation,

$$\nabla^2 F(\vec{r},\omega) + k^2 F(\vec{r},\omega) = 0, \tag{3}$$

where *F* is now capitalized to represent the space and frequency dependent oscillating variable, with the time dependence removed for brevity.

It is important to note the time dependence that is chosen by an author or software program when performing wavenumber processing. They are not all the same. For example, the Mathworks® software program MATLAB uses a time dependence of $e^{j\omega t}$ where the book *Sound, Structures, and Their Interaction* by Junger and Feit[5] uses a time dependence of $e^{-j\omega t}$. Both of these time dependencies are acceptable, but must be properly connected to the appropriate sign convention of the wavenumber (more on this below).

2.2 Time to Frequency

The above mentioned sign convention for solutions to the wave equation also dictates the form of the Fourier transform pairs: time-frequency and space-wavenumber. Using the $e^{j\omega t}$ time convention the time-frequency Fourier transform pair becomes

$$F(\omega) = \int_{-\infty}^{\infty} f(t) e^{-j\omega t} dt, \tag{4}$$

$$f(t) = \frac{1}{2\pi}\int_{-\infty}^{\infty} F(\omega) e^{j\omega t} d\omega, \tag{5}$$

where Equation 4 is the temporal Fourier transform and Equation 5 is the inverse temporal Fourier transform. Frequency spectra, by definition, are complex and two-sided, but symmetrically identical about 0 frequency. Since negative frequency isn't useful, we simply double the positive terms,

[1] Homogeneous means no sources (the differential equation is equal to zero).

and report single-sided spectra. This maintains the correct total energy in the time domain signal, but eliminates the nonsensical negative frequencies. Figure 1 shows the temporal Fourier transforms for a 500 Hz decaying sine wave (left) and random noise (right). Both the double- and single-sided linear spectra are shown in magnitude and phase. Here you can observe that the magnitude is doubled in the single-sided spectra, and we ignore the negative frequency component. As expected, the phase for the random signal is also randomized in the frequency domain. So far, so good - most beginning acousticians have little trouble with time-frequency transformations.

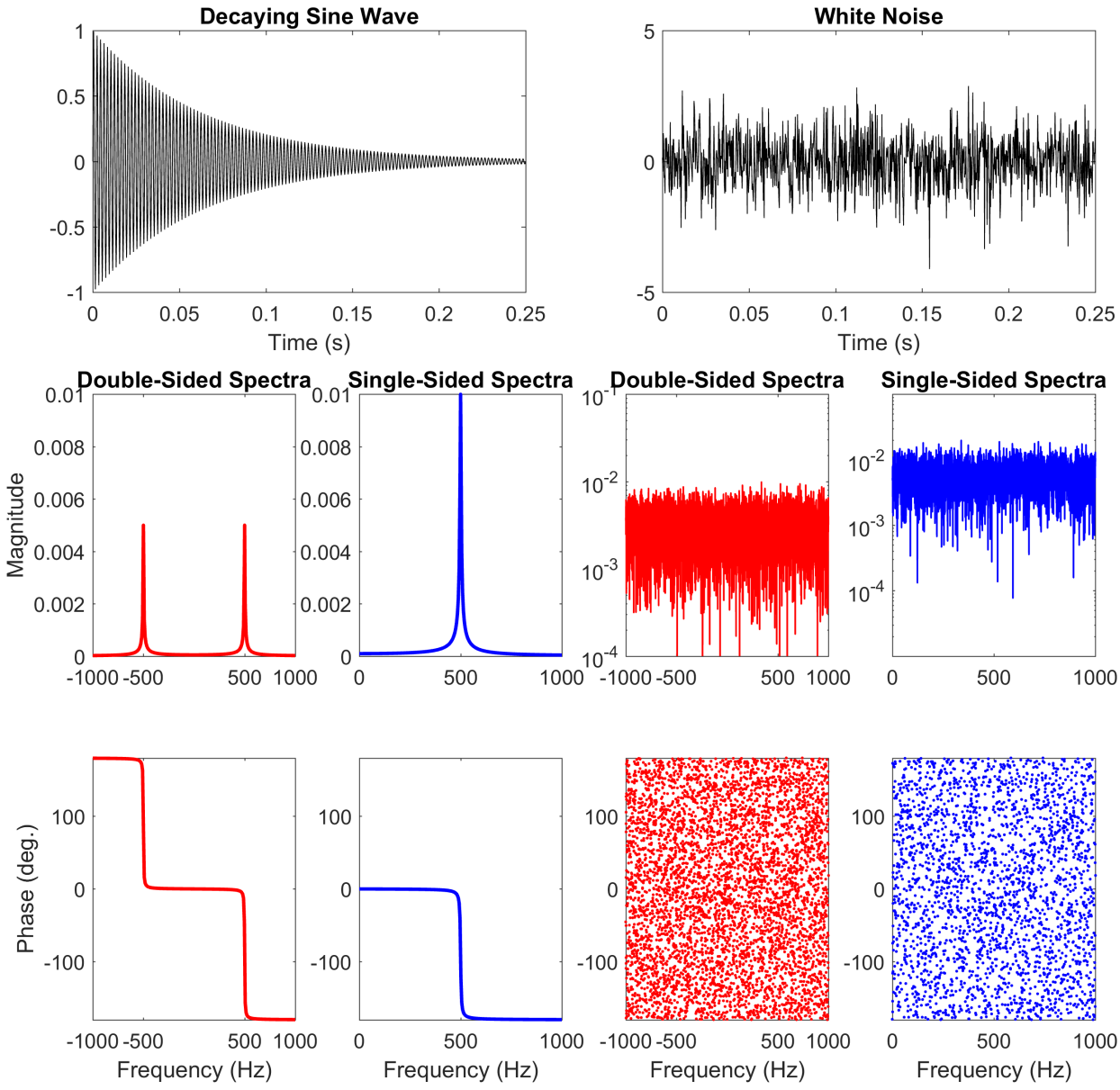

Fig. 1 – Time (top) and frequency (bottom) representation of a 500 Hz decaying sine wave (left) and random noise (right). Both double-sided (columns 1 and 3) and single-sided (columns 2 and 4) linear spectra are shown in magnitude (middle row) and phase (bottom row).

2.3 Space to Wavenumber

Analogous to the time-frequency Fourier transform pair in Equations 4 and 5, the space-wavenumber Fourier transform pair becomes

$$F(k) = \int_{-\infty}^{\infty} f(\vec{r}) e^{j\vec{k}\cdot\vec{r}} d\vec{r}, \tag{6}$$

$$f(\vec{r}) = \frac{1}{2\pi} \int_{-\infty}^{\infty} F(k) e^{-j\vec{k}\cdot\vec{r}} dk, \tag{7}$$

where Equation 6 is the spatial Fourier transform, or wavenumber transform, and Equation 7 is the inverse spatial Fourier transform, or inverse wavenumber transform. It is easy to observe the similarities between Equations 4 and 6 and Equations 5 and 7, respectively. The operating variables have changed from time-frequency to space-wavenumber and the kernel now operates on *kr*, rather than ωt. The final important difference is that the sign of the exponent in the space-wavenumber transform kernel is opposite that of the time-frequency transform. This is also a consequence of the choice of time dependence from section 2.1. If you select the other time dependence, the sign on all the kernel exponents should be reversed from what is shown in this tutorial.

Now consider a single wave propagating from left to right in an infinite beam at frequency *f* as shown in Figure 2[2]. By definition, the wave is defined by a single wavenumber $k = \omega/c$, where ω is radial frequency and *c* is wavespeed, and the wavenumber transform is a single peak, similar to what we observed for the tonal component of the time-frequency example. Here is the first major difference between space-wavenumber and time-frequency transforms: spatial vibrations can include right and left traveling waves, whereas we ignore negative time travel in the time domain. This is also why we like to choose the time dependence of $e^{j\omega t}$: positive wavenumbers represent rightward (or outward) traveling waves. If we had chosen the other time dependence, positive wavenumbers would represent leftward (or inward) traveling waves. Figure 3 adds a left traveling wave to the beam, and a negative wavenumber peak appears in the transform.

Finally, consider a finite beam with left and right traveling waves reflecting off of its edges. This adds the concept of spatial windowing to our discussions. This is analogous to windowing a time history with a 'boxcar' window. The sudden truncation of the vibration field scatters the wavenumber distribution into many additional terms, as shown in Figure 4. This distribution, once again, includes positive and negative wavenumber components. The distribution shown in Figure 4 is that of a *mode shape*, where the left and right waves constructively interfere over a finite distance to form a seemingly standing wave pattern. The wavenumber transform reveals that the standing wave pattern is actually comprised of left and right traveling waves.

[2]If you don't see the wave propagating in this PDF, search for the lead author on the internet, visit my personal website, and download a version which includes the animations.

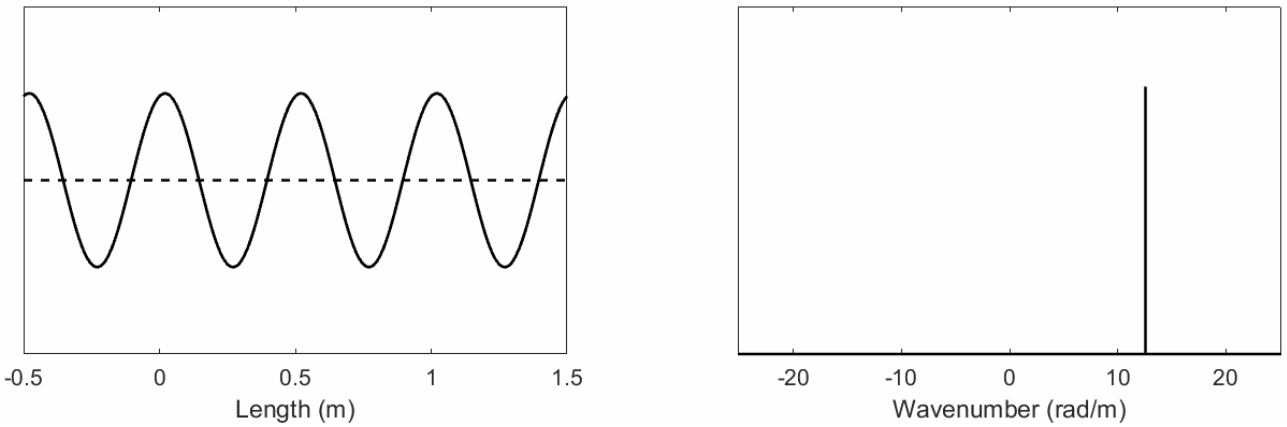

Fig. 2 – Left - right propagating wave in an infinite beam; Right - Wavenumber transform

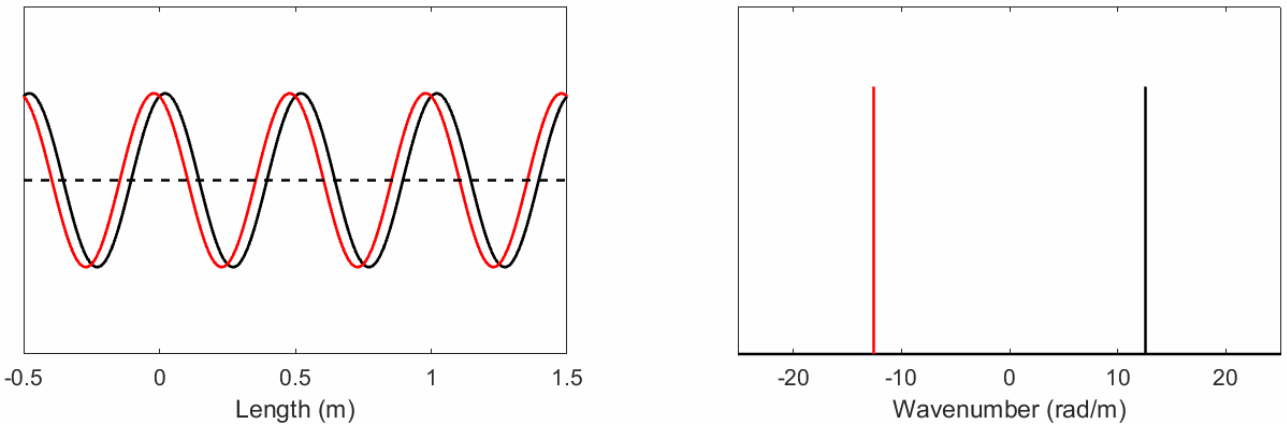

Fig. 3 – Left - Left and right propagating waves in an infinite beam; Right - Wavenumber transform

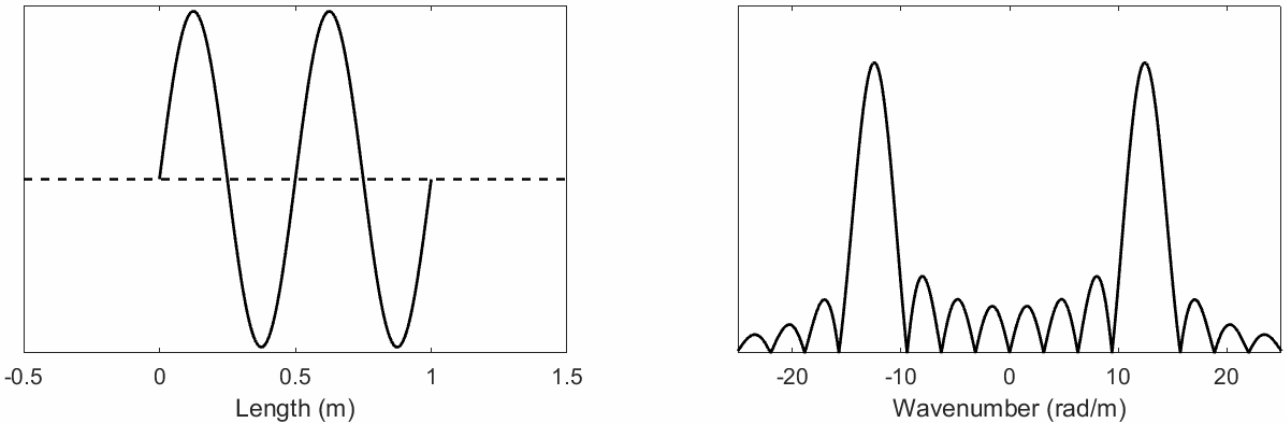

Fig. 4 – Left - Standing wave in a finite beam; Right - Wavenumber transform

3 TWO-DIMENSIONAL TRANSFORMS

3.1 Simply supported plate modes and simple filtering

Consider now vibration waves that also travel forward and backward in a two-dimensional flat plate (along the y-axis here). Although rarely found in practice, we continue the time-honored tradition of examining modes of vibration in a simply supported rectangular flat plate. Figure 5 shows the (4,2) mode[3] of the 229 mm x 127 mm x 6 mm steel rectangular panel analyzed in Barnard and Hambric[6]. Now our spatial transforms are two dimensional, and usually shown as a contour map. Also, although the wavenumber transform allows for positive and negative amplitudes, it is common to show the power spectrum of the transform, which is simply the square of the magnitude.

One of the benefits of wavenumber transforms is the use of filtering. Selected ranges of wavenumber may be retained or removed, and the filtered wavenumber response inverse transformed back to space. Later, we will explore how this methodology may be used to identify the radiating components of a structural vibration field. For now, we demonstrate simple filters like removing all left traveling wavenumber components (negative k_x), as shown in Figure 6. We can also remove backward traveling components (negative k_y) as shown in Figure 7. This PDF includes animations, so if you're reading this on a computer you should be able to easily visualize the effects of the filtering on the spatial vibration patterns[4].

3.2 Supersonic vibrations (acoustic radiation)

So far, we have only considered transforms of vibration patterns without regard to underlying structural properties and wavespeeds. This is because these transforms are of spatial distributions, and therefore depend only the vibration pattern. Now we superimpose the acoustic wavenumber on our wavenumber transform plots of the (9,6) mode at a specific frequency (2500 Hz) in Figure 8. All low-wavenumber components inside the 'radiation circle' are supersonic; high wavenumber components are subsonic, or evanescent, and do not radiate sound. For this low frequency (below the coincidence frequency of bending waves in the plate) filtering the subsonic (high wavenumber) terms and inverse transforming reveals the well-known corner radiator pattern described by many authors (for example see Fahy[7] or Hambric, Nefske, and Sung[8]). This filtering is the basis of the field of Acoustic Holography[9] and other similar methods[10].

Raising frequency increases wavenumber, and the size of the radiation circle so that it encompasses more of the wavenumber content of the vibration pattern. Figure 9 shows the condition where waves traveling in the y direction are supersonic (the circle extends beyond the dominant k_y peaks) but those traveling in the x-direction are subsonic. The so-called 'line' or 'edge' radiators of this mode type are visible in the inverse transformed mode shape. Though not shown here, the case with very high acoustic wavenumber simply converges to the unfiltered mode shape.

3.3 Structure-borne sound transmission

Wavenumber analysis may also be used to estimate the structure-borne sound transmission coefficients between connected plates. Transmission coefficients are necessary for Statistical Energy Analysis (SEA) of interconnected structures. Hambric and Barnard[11] describe two honeycomb

[3]The indices (m, n) indicate the number of half waves along the x and y axis of the plate.

[4]If the animations don't work in this PDF, search for the lead author on the internet, visit my personal website, and download a version with the animations.

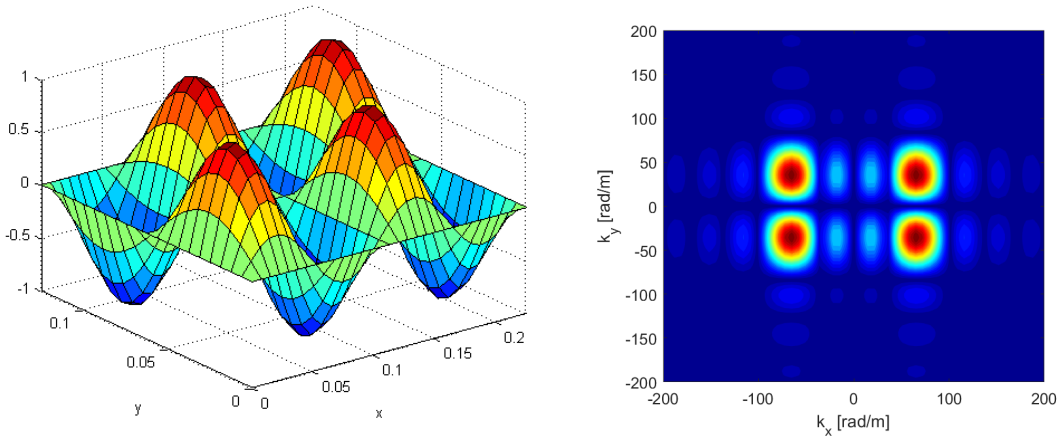

Fig. 5 – Structural mode shape (left) and power spectrum of wavenumber transforms of (4,2) mode

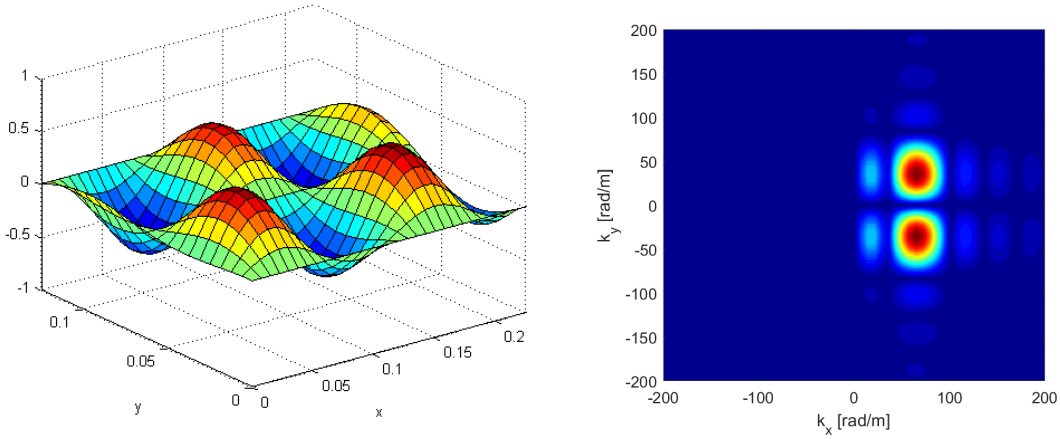

Fig. 6 – Structural mode shape (left) and power spectrum of wavenumber transforms of (4,2) mode with only positive k_x components

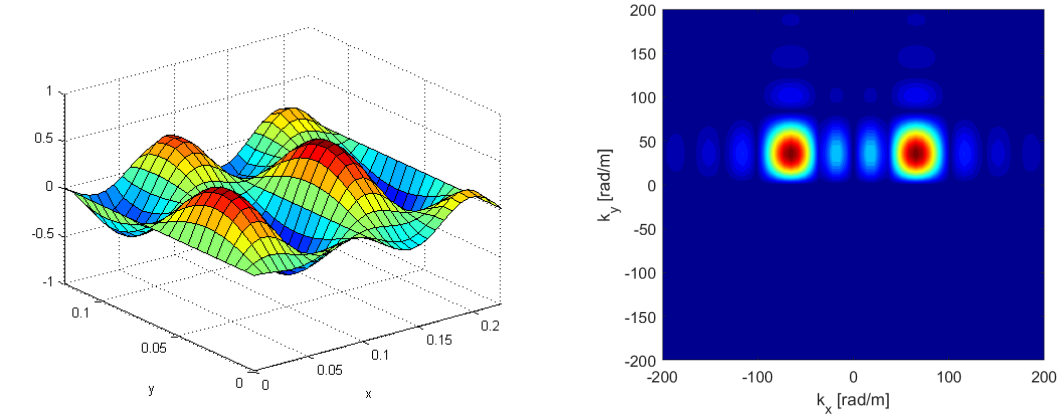

Fig. 7 – Structural mode shape (left) and power spectrum of wavenumber transforms of (4,2) mode with only positive k_y components

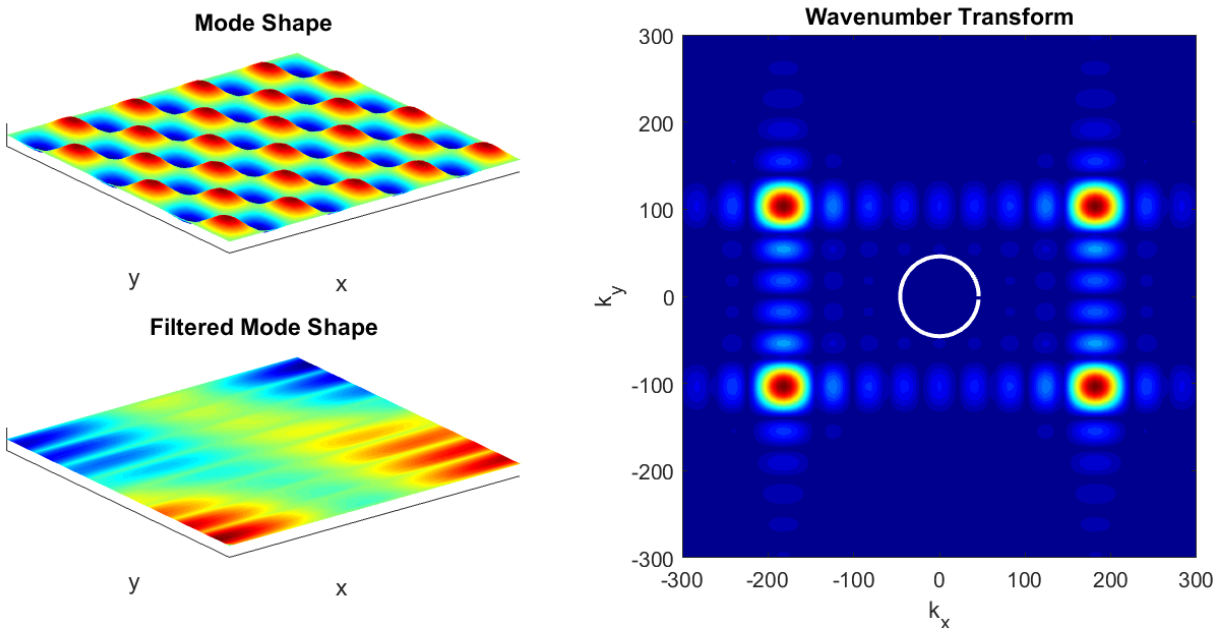

Fig. 8 – Right: wavenumber transform of (9,6) mode shape with acoustic wavenumber circle at a frequency below coincidence; Left top - original mode shape; Left bottom - inverse transform of supersonic wavenumber components

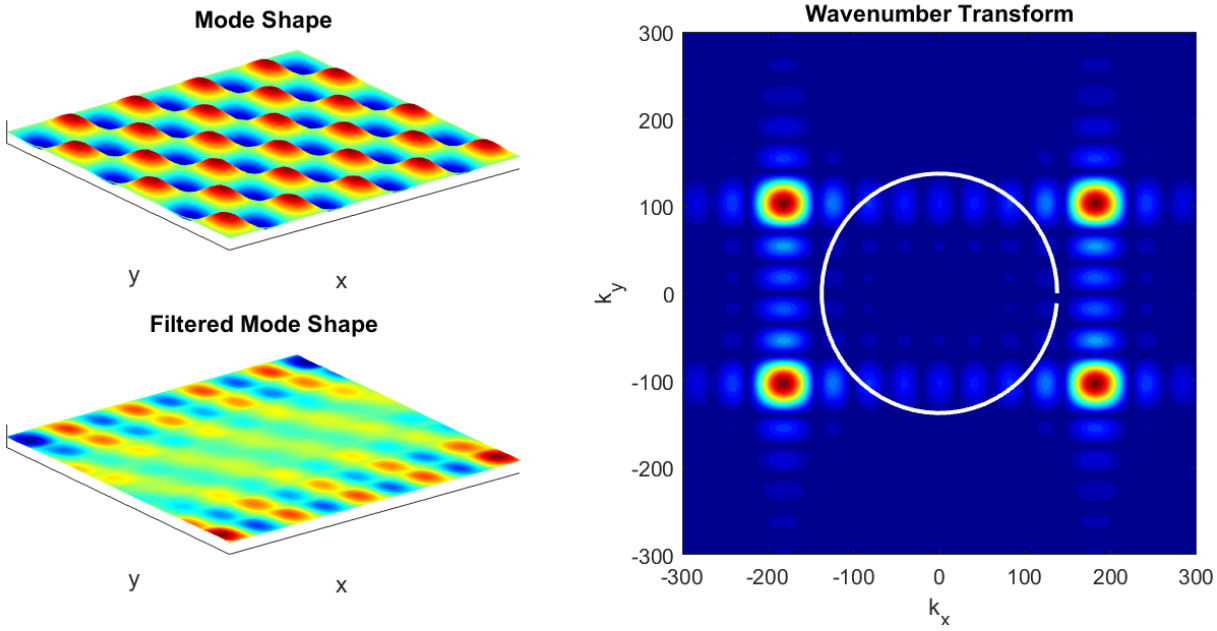

Fig. 9 – Right: wavenumber transform of (9,6) mode shape with acoustic wavenumber circle at a frequency near coincidence; Left top - original mode shape; Left bottom - inverse transform of supersonic wavenumber components

core carbon-fiber facesheet sandwich panels bolted along a common edge (see Figure 10). The panels were suspended vertically from soft cords and experimental modal analyses conducted. Accelerometers mounted to the panel served as reference locations, where through reciprocity they become source locations. Both panels were repeatedly struck over a dense rectangular grid of locations with an instrumented force hammer to measure frequency response functions (FRFs) between the panel surfaces and the source/reference locations. These rectangular grids of FRF distributions were transformed to wavenumber space.

The transforms were filtered in two ways. First, the energy within one-third octave (OTO) frequency bands was calculated. Second, the energy within a given OTO band was further filtered into its forward (with amplitudes *A*) and backward (with amplitudes *B*) propagating terms so that the vibration transmission coefficients between the 1st and 2nd plates could be calculated using the well-known formulas:

$$\tau_{12}(f) = \frac{D_2|B_2|^2}{D_1|B_1|^2} \quad \text{and} \quad \tau_{21}(f) = \frac{D_1|A_1|^2}{D_2|A_2|^2}, \tag{8}$$

where the *D* terms are the flexural rigidities of panels 1 and 2.

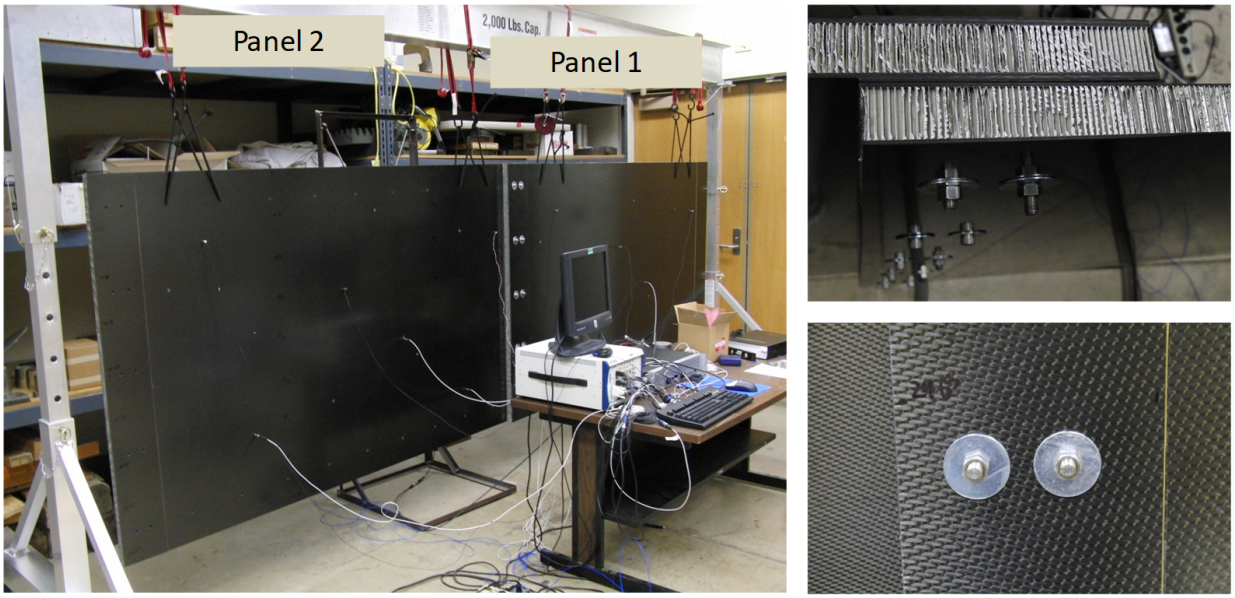

Fig. 10 – Sandwich panels bolted along middle edge described in [11].

Figure 11 shows the wavenumber energy in the 1600 Hz OTO band for both panels for a drive location on panel 1, including forward filtered (right propagating waves only, filtering out negative k_x components) and backward filtered (left propagating waves only, filtering out positive k_x components). Since panel 1 is driven in this example, its vibration levels are higher. These filtered transforms are then integrated over all k_x and k_y to compute total amplitudes, and then used to compute the transmission coefficients shown in Figure 12 (note that τ_{12} is computed for reference drives on panel 1, and τ_{21} using reference drives on panel 2). The transmission coefficients range from 0.2-0.5 for frequencies up to where $k_b dL = \pi$. This corresponds to the frequency where a half structural wavelength spans the spacing between bolts along the edge. Note that another useful feature of wavenumber analysis is non-dimensionalizing wavenumber (with units 1/length) by multiplying by a characteristic length. By choosing length as the spacing between bolts, we can assess the physical wavelengths where the structure-borne transmission decreases. Here, the transmission decreases significantly above $k_b dL = \pi$.

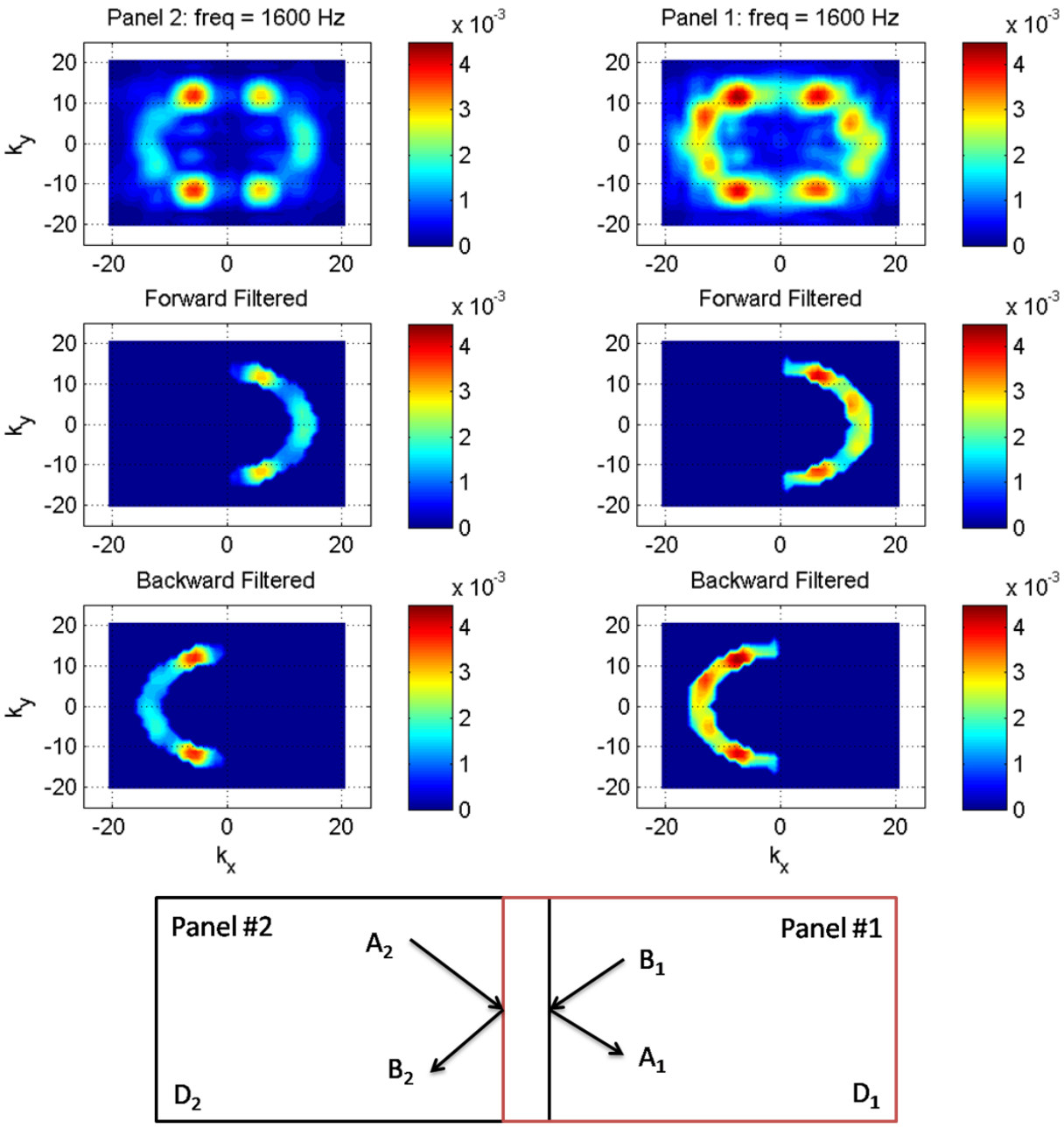

Fig. 11 – Wavenumber transforms of 1600 Hz OTO energy for both panels described in [11]. Top - total energy; middle - right propagating energy (from panel 2 to 1); bottom - left propagating energy (from panel 1 to 2).

4 SUMMARY

In this tutorial we have hopefully demystified wavenumber transforms of structural vibration fields by showing the similarity of a simple one-dimensional transform to that of time-frequency transforms. We have also emphasized the importance of knowing your time dependency, a step that is easily overlooked and can lead to misinterpreted results. We then added the concepts of left and right traveling waves, spatial windowing (finite structures), and two-dimensional structures. Finally, we showed how filtering may be used to assess acoustic radiation and structure-borne sound transmission. There are many other applications of wavenumber transforms that we didn't have space to include here, including how structures respond to flow-induced excitation. For more on that topic, see Hambric[12] and Hambric, Hwang, and Bonness[13].

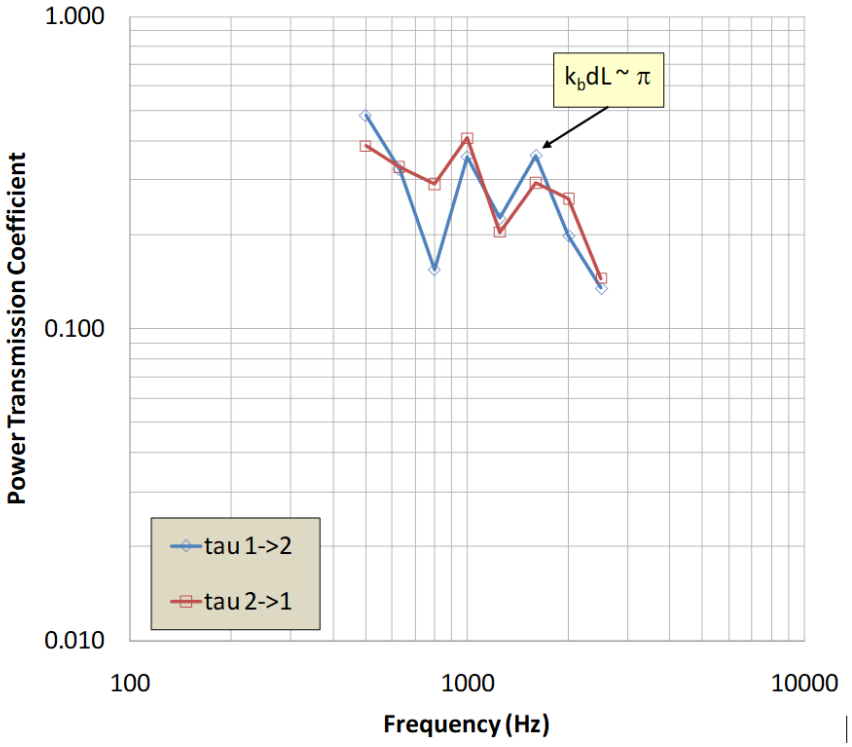

Fig. 12 – Structure borne power transmission coefficients computed using filtered wavenumber transforms of FRF fields on panels described in [11].

5 REFERENCES

1. S. Hambric, "Structural acoustics tutorial - part 1: Vibrations in structures," *Acoustics Today*, vol. 2, no. 2, 2006.

2. S. Hambric and J. Fahnline, "Structural acoustics tutorial - part 2: Sound-structure interaction," *Acoustics Today*, vol. 3, April 2007.

3. S. Hambric, "Tutorial on infinite panel sound transmission loss simulations," in *Proceedings of Internoise 2015*, August 2015. San Francisco, California, USA.

4. S. Hambric, "Tutorial on the vibroacoustics of composite sandwich panels," in *Proceedings of Internoise 2016*, August 2016. Hamburg, Germany.

5. M. Junger and D. Feit, *Sound, Structures, and their Interaction*. Acoustical Society of America, second ed., 1993.

6. A. Barnard and S. Hambric, "Development of a set of structural-acoustic teaching demonstrations using a simply supported rectangular plate," *Noise Control Engineering Journal*, vol. 64, pp. 500–510, July-August 2016.

7. F. Fahy and P. Gardonio, *Sound and Structural Vibration*. Academic Press, second ed., 2007.

8. S. Hambric, D. Nefske, and S. Sung, *Engineering Vibroacoustic Analysis: Methods and Applications*. Wiley, 2016.

9. E. Williams, *Fourier Acoustics: Sound Radiation and Nearfield Acoustical Holography*. Academic Press, 1999.

10. A. Barnard, S. Hambric, and J. Maynard, "Underwater measurement of narrowband sound power and directivity using supersonic intensity in reverberant environments," *Journal of Sound and Vibration*, vol. 331, pp. 3931–3944, 2012.

11. S. Hambric, A. Barnard, and S. Conlon, "Power transmission coefficients based on wavenumber processing of experimental modal analysis data for bolted honeycomb sandwich panels," in *Proceedings of Internoise 2010*, June 2010. Lisbon, Portugal.

12. S. Hambric and et. al., "I-INCE symposium report: Second symposium on flow-induced noise and vibration issues and aspects (FLINOVIA II)," in *Proceedings of Internoise 2017*, August 2017. Hong Kong.

13. S. Hambric, Y. Hwang, and W. Bonness, "Vibrations of plates with clamped and free edges excited by low-speed turbulent boundary layer flow," *Journal of Fluids and Structures*, vol. 19, no. 1, pp. 93–110, 2004.